Theory for the Ablation of Fiberglas-Reinforced Phenolic Resin

RONALD E. ROSENSWEIG*
Massachusetts Institute of Technology, Cambridge, Mass.

AND

NORMAN BEECHER†
National Research Corporation, a subsidiary of Norton Company, Cambridge, Mass.

A model is presented to describe stagnation point ablation for an axially symmetric body consisting of a heterogeneous dispersion of carbon particles in glass. Ablation for this system approximates important dynamic ablation characteristics of Fiberglas-reinforced phenolic resin materials. Endothermic carbon-silica reaction enters as a significant mechanism of ablation and produces a sharp cutoff temperature for any given stagnation point pressure, thus giving rise to a surface-adjacent zone where all chemical reaction occurs. Other processes encompassed in the mathematical model are energy transport, molten glass flow, and mass addition to the boundary layer. Numerical results are in encouraging agreement with experiment.

Nomenclature

a,b = constants in viscosity relationship for the melt
c_p = specific heat of ablation material
ΔE = activation energy of chemical reaction
h_i = gas enthalpy evaluated at wall temperature
h_s = stagnation enthalpy of gas outside the boundary layer
ΔH = enthalpy change of chemical reaction
k = thermal conductivity
k_R = chemical kinetic rate coefficient
K_a = equilibrium constant
$\dot{m}$ = rate of mass addition to the boundary layer
n = a/T, a viscosity parameter
p = pressure
p_{CO} = partial pressure of carbon monoxide
p_s = stagnation pressure
q = heat flux
q_0 = heat flux to nonablating surface
r = radius measured from centerline
R = nose cone radius; also ideal gas constant
T = temperature within the melt
T_0 = temperature of ablation material before heating
T_R = temperature within reaction zone
T_s = surface temperature
u = velocity along x direction
u_e = gas velocity in x direction at edge of boundary layer
u_i = velocity at interface between melt zone and reaction zone
v = velocity in y direction
v_i = velocity at melt-zone, reaction-zone interface
v_∞ = ablation velocity
x = distance from stagnation point measured perpendicular to the centerline
y = coordinate normal to the surface
α = activity coefficient of chemical species
δ = characteristic thickness of melt zone
δ_R = thickness of reaction zone
δ_T = thermal thickness; defined by Eq. (13)
μ = viscosity
μ_i = viscosity at melt-zone, reaction-zone interface
μ_R = viscosity in reaction zone
ρ = density of melt
ρ_R = density of material in reaction zone
ρ_s = stagnation density of gas
σ_s = Prandtl number of gas
τ = shear stress
τ_0 = shear stress on nonablating wall
ψ = blowing factor

Received January 17, 1963; revision received June 18, 1963.
The authors wish to thank W. R. Lucas and C. O. Gray for their helpful comments. The assistance of personnel of the Army Ballistic Missile Agency, particularly E. Braunlich and E. T. Seely, in the machine computations is also acknowledged gratefully. This work was supported by the Army Ballistic Missile Agency under Contract DA-19-020-ORD-4689.

* Assistant Professor of Chemical Engineering; also Consultant to National Research Corporation; now with Avco Research and Advanced Development Division, Wilmington, Mass.
† Assistant Director of Research.

Introduction

THE ability of reinforced plastics to withstand extremely high heat flux for short periods has made possible their use for re-entry nose cones and rocket nozzles. Fiberglas-reinforced phenolic resins have been of great importance. The combined effects of heat and stress, termed ablation, involve the raising to a destructively high temperature of only a thin surface layer, whereas the bulk of the material suffers no thermal damage.

In an earlier communication,[1] the nature of the ablation process was described qualitatively based on experimental laboratory data and examination of ground and re-entry tested specimens. Those observations are used as the basis for the realistic model of re-entry ablation described below. It has been found possible to predict the overall ablation rate, surface temperature, and other characteristics of the actual ablation process to encouraging accuracy.

Description of the Ablation Model

Figure 1 is a diagram of the analytical model of ablation but with the thickness of the process zones greatly exaggerated. Coordinates are fixed in the surface so that under steady-state ablation conditions the material in all zones moves upward relative to the coordinates. $y = 0$ corresponds to a position on the outerline at the melt-layer, reaction-layer interface. Before reaching the melt zone, the raw plastic first passes through a zone of heating; this is followed by rapid pyrolysis into gases and solid residue. The gaseous products flow through the porous solid and molten glass and finally are injected into the gas boundary layer. The solid residue is a mixture of glass and carbonaceous material, which also moves upward. It gradually becomes molten and will flow under shear or pressure forces. A considerable portion of the material will flow away in the lateral direction before it reaches the surface, and the bulk of this flow occurs over the melt zone whose thickness is δ. The remainder of the material advances into the surface zone whose thickness is δ_R. In

this surface zone there is chemical reaction between carbon and glass, and additional gases are produced. There is competition between this inorganic reaction and lateral flow for the removal of material from this zone.

Processes considered in the analysis include 1) boundary-layer heat transfer, 2) heat blocking due to mass injection into the boundary layer, 3) reduction of shear due to mass injection to the boundary layer, 4) thermodynamic coupling between stagnation pressure and cutoff temperature for the carbon-glass reaction, 5) disappearance of material due to chemical reaction, 6) flow in the reaction portion of the melt, 7) flow in the nonreacting portion of the melt, 8) heat absorption due to chemical reaction, 9) heat transfer within the condensed phases, and 10) pyrolysis of organic material.

Development of the Theory

When subjected to aerodynamic heat transfer and shear forces, a glassy material will form a flowing liquid layer. Energy transferred to the material is absorbed in the form of heat capacity and latent heat of vaporization (for that fraction of the material which vaporizes). The ablation rate for this type of process was treated by Bethe and Adams[2] in a simplified though ingenious manner and by Sutton,[3] who numerically integrated the governing equations. Hidalgo,[4] in extending Bethe and Adams' treatment, points out that the numerical procedure is rather cumbersome and time-consuming for practical applications and that any approximate method of integration and appropriate simplification of the relevant equations have great practical importance. A similar philosophy is adopted here, and it is found possible to obtain a set of simultaneous algebraic equations that describe the ablation. These equations are found suitable for rapid solution by means of high-speed digital computation.

The development of the equations is presented next. The system is illustrated in Fig. 1.

Continuity Equations

For the melt zone at the stagnation region,

$$(\partial/\partial r)(ru) + r(\partial v/\partial y) = 0 \quad (1)$$

Likewise, for the reaction layer at the stagnation region, taking account of mass disappearance due to chemical reaction,

$$(\partial/\partial r)(ru) + r(\partial v/\partial y) + (rk_R/\rho_R)\exp(-\Delta E/RT_R) = 0 \quad (2)$$

Here the chemical reaction is pictured as simply

$$\text{condensed reactants} \rightarrow \text{gaseous products}$$

The reaction is considered irreversible and governed by a first-order kinetic description

$$\text{rate mass reacts/unit volume} = k_R \exp(-\Delta E/RT_R) \quad (3)$$

Inherent in Eq. (2) is the assumption that gases reach the surface with no holdup in the liquid. The validity of this rather crude assumption possibly is enhanced by the existence of a very thin reaction layer, the presence of which is borne out by the subsequent results. It is found that nearly all material entering the reaction layer undergoes reaction, and hence the accurate description of flow in this layer may not be critical.

Equation of Motion

The equation of motion is for viscous flow over an axially symmetric body with pressure gradient and has the same form for both the melt zone and the reaction layer:

$$-(\partial p/\partial r) + (\partial/\partial y)[\mu(\partial u/\partial y)] = 0 \quad (4)$$

Although this equation is reasonably valid for the melt zone, its usefulness for describing flow in the reaction zone is impaired to an unknown degree by the nonhomogeneity of the flow. Nonetheless, it is believed that useful results will be obtained and that trends will remain unchanged.

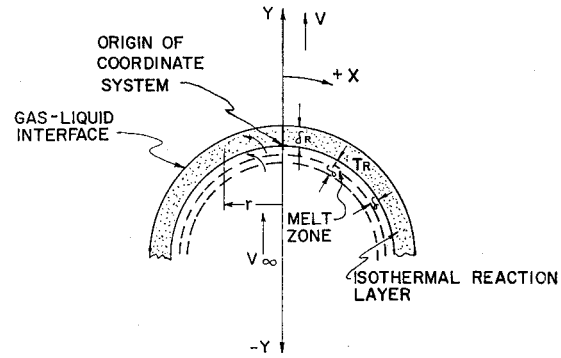

Fig. 1 Diagram of ablation model.

Energy Equation

This equation describes the balance between convective transport of enthalpy and thermal conduction of heat. It is assumed that lateral conduction of heat is unimportant. For a quasi-one-dimensional system wherein velocity may be a function of y, there is obtained

$$v(\partial T/\partial y) = (k/\rho c_p)(\partial^2 T/\partial y^2) \quad (5)$$

No energy equation is required for the reaction zone if it is assumed that the zone is isothermal at T_R, the reaction temperature. This assumption, good for a thin zone, is enhanced further since, in addition, the endothermic reaction tends to maintain constant temperature; hence this assumption is adopted.

Integration of Equations

It is found possible to integrate the foregoing equations by making some further approximations, and, as a result, the partial differential equations are converted to a system of simultaneous algebraic equations.

The energy equation (5) is integrated by considering v to be constant throughout the melt zone and equal to the velocity v_∞ at which solid material moves toward the reaction zone. With boundary conditions of $T = T_0$ at $y = -\infty$ and $T = T_R$ at $y = 0$, there results

$$(T - T_0)/(T_R - T_0) = \exp[(v_\infty \rho c_p/k)y] \quad (6)$$

Integration of (4) gives an equation relating local velocity gradient to position in the melt layer:

$$\mu(\partial u/\partial y) = p'y + C_1$$

where $p' = \partial p/\partial x$. The constant will be determined by requiring continuity of shear at the reaction-layer, melt-zone interface, but first the reaction-layer-integrated form of (4) is required. In this case $\mu = \mu_R$ and is constant:

$$\mu_R(\partial u/\partial y) = p'y + C_2$$

At $y = \delta_R$, $\tau = \mu_R(\partial u/\partial y)$, where τ is shear at the wall and will be evaluated from gas boundary-layer considerations but is for present considered as a "known." This gives $C_2 = (\tau - p'\delta_R)$ and hence

$$\mu_R(\partial u/\partial y) = p'y + (\tau - p'\delta_R)$$

A second integration over y relates velocity to position in the reaction layer:

$$\mu_R u = (p'y^2/2) + (\tau - p'\delta_R)y + C_3$$

The constant C_3 is evaluated by setting $u = u_i$ at $y = 0$, and this gives

$$\mu_R u = (p'y^2/2) + (\tau - p'\delta_R)y + \mu_R u_i \tag{7}$$

Setting $y = \delta_R$ provides an expression for surface velocity u_w in terms of interface velocity u_i:

$$u_w = (\tau\delta_R/\mu_R) - (p'\delta_R^2/2\mu_R) + u_i \tag{8}$$

Next the interfacial shear is evaluated from (7):

$$\mu(\partial u/\partial y)_{y=0+} = \tau - p'\delta_R$$

This determines C_1 to be $C_1 = \tau - p'\delta_R$, and the melt equation becomes

$$\mu(\partial u/\partial y) = p'y + (\tau - p'\delta_R)$$

Thus the following integration is required:

$$\int_0^{u(y)} du = p' \int_{-\infty}^{y} \frac{y\,dy}{\mu} + (\tau - p'\delta_R) \int_{-\infty}^{y} \frac{dy}{\mu} \tag{9}$$

To integrate Eq. (9), the viscosity-temperature relationship must be specified. Viscosity of Fiberglas E, pyrex, and presumably many other glasses are described by the following formula:

$$\mu = \exp[(a/T) - b]$$

This relationship is used later to compute viscosity at the surface. An approximation is used to relate viscosity of cooler material under the surface relative to the surface viscosity. The exact expression for relative viscosity is independent of the constant b:

$$\mu/\mu_R = \exp\{a[(1/T) - (1/T_R)]\}$$

As an approximation that is more convenient for subsequent integration,

$$\mu/\mu_R \cong (T/T_R)^{-a/T} \tag{10}$$

The suitability of the alternate form may be judged from examining leading terms:

$$a\left(\frac{1}{T} - \frac{1}{T_R}\right) = -\frac{a}{T}\ln\frac{T}{T_R}$$

$$= -\frac{a}{T}\left[\frac{T - T_R}{T_R} - \frac{1}{2}\left(\frac{T - T_R}{T_R}\right)^2 + \cdots\right]$$

Equality results if the higher order terms are negligible. Thus, a criterion is that

$$2T_R/(T_R - T) > 1 \tag{11}$$

which results from ratioing the first two terms in the log expansion; the ratio varies from infinity at $y = 0$ to about 2 at $y = -\infty$ and is judged acceptable. For small T_0, Eq. (6) gives

$$T/T_R = \exp[v_\infty \rho c_p/k]y = \exp(y/\delta_T) \tag{12}$$

where δ_T measures the extent of heat penetration into the melt corresponding to a reduction in T/T_R of $1/e$ and will be called the thermal thickness:

$$\delta_T = (k/v_\infty \rho c_p) \tag{13}$$

From (12) and (10), a simple equation results which relates viscosity to position and implicitly allows for temperature variation throughout the material:

$$\mu/\mu_R = \exp(-yn/\delta_T) = \exp(-y/\delta) \tag{14}$$

The viscosity-temperature relationship actually used is appropriate for Fiberglas and reads

$$\mu = \exp[(30{,}000/T) - 13]$$

where μ is in poises and T is degrees Kelvin.

In Eq. (14), $n = a/T$ (will be assigned an average value), and $\delta = \delta_T/n$ appropriately is termed the liquid thickness. For materials of interest, $n > 1$, and the liquid thickness is less than thermal thickness. It will be seen that this insures that chemical reaction occurs in molten material; chemically induced rupture of solid material therefore is not a factor.

Equation (9) now may be integrated with the substitution of Eq. (14) to give an expression for velocity in the melt zone:

$$u(y) = \frac{p'}{\mu_R}\left(\frac{\delta_T}{n}\right)^2\left(\frac{n}{\delta_T}y - 1\right)\exp\left(\frac{ny}{\delta_T}\right) + \left(\frac{\tau - p'\delta_R}{\mu_R}\right)\frac{\delta_T}{n}\exp\left(\frac{ny}{\delta_T}\right) \tag{15}$$

It may be noted that this equation reduces to Eq. (12) of Bethe and Adams[2] for $\delta_R = 0$. Equation (15) provides another expression for u_i by setting $y = 0$:

$$u_i = -\frac{p'}{\mu_R}\left(\frac{\delta_T}{n}\right)^2 + \left(\frac{\tau - p'\delta_R}{\mu_R}\right)\frac{\delta_T}{n} \tag{16}$$

The prime interest is in obtaining an expression for v_∞. To achieve this, consider the v component of velocity in its relation to the u component by means of the continuity equation (1). Symbolically integrating over y at fixed x gives

$$\int_{v_\infty}^{v_i} dv = -\frac{1}{r}\int_{-\infty}^{0} \frac{\partial}{\partial r}(ur)\,dy \tag{17}$$

In the near vicinity of a stagnation point, $r = x$ so that (17) becomes

$$v_i - v_\infty = -\frac{1}{x}\int_{-\infty}^{0} u\,dy - \int_{-\infty}^{0} \frac{\partial u}{\partial x}\,dy \tag{18}$$

With the help of (15), the first integral may be evaluated:

$$\int_{-\infty}^{0} u\,dy = -2\frac{p'}{\mu_R}\left(\frac{\delta_T}{n}\right)^3 + \left(\frac{\tau - p'\delta_R}{\mu_R}\right)\left(\frac{\delta_T}{n}\right)^2 \tag{19}$$

Although this integral is of infinitesimal order for integration along the centerline, its ratio to x is a finite quantity:

$$\int_{-\infty}^{0} \frac{\partial u}{\partial x}\,dy = -2\left(\frac{\delta_T}{n}\right)^3\frac{p''}{\mu_R} - \left(\frac{\delta_T}{n}\right)^2\delta_R\frac{p''}{\mu_R} + \left(\frac{\delta_T}{n}\right)^2\frac{\tau'}{\mu_R} \tag{20}$$

In forming $\partial u/\partial x$ to obtain Eq. (20), use has been made of the following conditions:

$$(\partial\delta_T/\partial x)_{y=0} = 0 \qquad (\partial\delta_R/\partial x)_{y=0} = 0$$

These conditions should apply reasonably at a stagnation point due to the symmetry involved.

Combining (18–20) gives an equation relating velocity v_i at which material flows into the reaction layer to system parameters:

$$v_i - v_\infty = 4\frac{p''}{\mu_R}\left(\frac{\delta_T}{n}\right)^3 - 2\frac{\tau'}{\mu_R}\left(\frac{\delta_T}{n}\right)^2 + 2\frac{p''\delta_R}{\mu_R}\left(\frac{\delta_T}{n}\right)^2 \tag{21}$$

It may be noted that, for $\delta_R = 0$, this reduces to Eq. (14) of Bethe and Adams,[2] their "fundamental" equation. In this development it still is necessary to eliminate mention of v_i, which can be done by considering the distribution of velocities in the reaction zone. Thus, from the continuity equation for the reaction layer [Eq. (2)], there is obtained by integrat-

ing over y at $x = 0$

$$-\int_{v_i}^{0} dv = \frac{1}{x}\int_0^{\delta_R} \frac{\partial}{\partial x}(ux)\,dy + \frac{k_R\delta_R}{\rho_R}\exp\left(-\frac{\Delta E}{RT_R}\right) = v_i \tag{22}$$

The integration limit $v = 0$ at $y = \delta_R$ implies no surface vaporization effects. It does not, however, preclude gas injection into the gas boundary layer. In fact, injection of inorganic reaction product gases and resin pyrolysis gases will be included in this model. The former are produced within the reaction zone volume, whereas the latter are produced within the underlying solid material. Hence, neither would result in a finite velocity v for the melt at $y = \delta_R$. Using Eq. (7) to substitute for u in (22) gives, after some calculations and with use of (16) for u_i, an expression for v_i which is independent of Eq. (21):

$$v_i = \frac{p''\delta_R^3}{3\mu_R} + \left(\frac{\tau' - p''\delta_R}{\mu_R}\right)\delta_R^2 - \frac{2}{\mu_R}\delta_R p''\left(\frac{\delta_T}{n}\right)^2 + \frac{2}{\mu_R}\delta_R(\tau' - p''\delta_R)\frac{\delta_T}{n} + \frac{k_R\delta_R}{\rho_R}\exp\left(-\frac{\Delta E}{RT_R}\right) \tag{23}$$

Eliminating v_i between (23) and (21) provides the following equation for v_∞:

$$v_\infty = p''\left[-\frac{2}{3}\frac{\delta_R^3}{\mu_R} - \frac{2}{\mu_R}\delta_R^2\frac{\delta_T}{n} - \frac{4\delta_R}{\mu_R}\left(\frac{\delta_T^2}{n}\right) - \frac{4}{\mu_R}\left(\frac{\delta_T}{n}\right)^2\right] + \tau'\left[\frac{\delta_R^2}{\mu_R} + 2\frac{\delta_R\delta_T}{\mu_R n} + \frac{2}{\mu_R}\left(\frac{\delta_T}{n}\right)^2\right] + \frac{k_R\delta_R}{\rho_R}\exp\left(-\frac{\Delta E}{RT_R}\right) \tag{24}$$

Again, this reduces to (14) of Bethe and Adams[2] for $\delta_R = 0$ and $v_i = 0$. As it stands, Eq. (24) is effectively a relationship between v_∞, δ_R, and T_R, and thus two additional relationships are needed in order to set the complete solution. One of the additional relationships results from an overall heat balance applied to the system bounded by a small surface area of the reaction zone at the stagnation point and having δ_R thickness. With the temperature base of enthalpy reckoned at T_R, no terms result from lateral convection of fluid (all at T_R) or from vapor removal (all at T_R), so that heat added to the surface from the boundary layer, q, equals heat absorbed by reaction plus heat conducted out into the melt zone:

$$q = v_\infty \rho c_p(T_R - T_0) + \delta_R k_R \exp(-\Delta E/RT_R)\,\Delta H \tag{25}$$

Use of v_∞ in Eq. (25) involves some approximation, since not all the underlying melt that becomes ablated is heated to T_R. The adequacy of this approximation can be evaluated by use of the temperature profile nearly valid in the material that previously was given as Eq. (12):

$$T = T_R\exp(y/\delta_T) = T_R\exp(y/n\delta)$$

where δ is the liquid thickness and appeared in Eq. (14). The temperature drop ΔT across the liquid layer is therefore

$$\Delta T = T_R\{1 - \exp[-(1/n)]\} \tag{26}$$

Recalling that $\exp(x) = 1 + x + (x^2/2) + \ldots$ and noting that n is a large number, about 16, it is seen that $\Delta T \cong T_R/n$. Since the material moves up with velocity v_∞ to temperature $T_R[1 - (1/n)] \cong \frac{15}{16}\,T_R$ before appreciable melting and lateral flow occur, it is concluded that use of v_∞ leads to only a few percent error.

Chemical Relationships

Equations (25) and (24) supply two relationships in the three unknowns T_R, v_w, and δ_R, and clearly another relationship must be found. So far the existence of the reaction layer only has been assumed, and it is in the proof of this assertion that the other required equation is to be found.

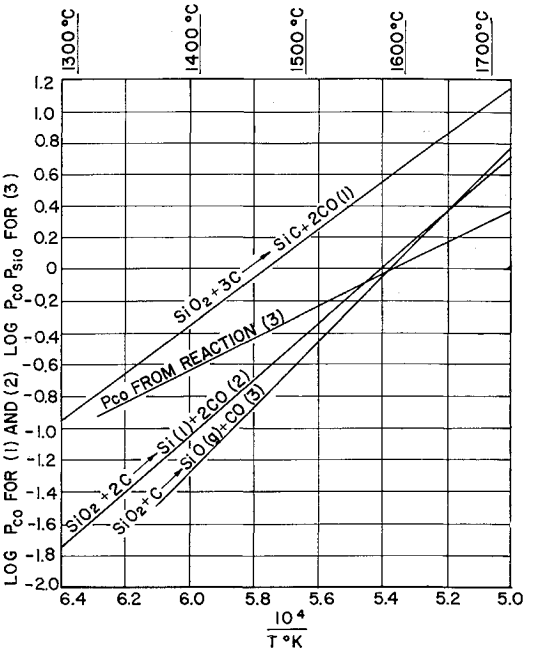

Fig. 2 Equilibria in reactions between silica and carbon.

Three reactions of carbon with silica appear to be of possible importance. They are

$$SiO_2 + 3C \rightarrow SiC + 2CO \tag{27}$$

$$SiO_2 + 2C \rightarrow Si\ (l) + 2CO \tag{28}$$

$$SiO_2 + C \rightarrow SiO\ (g) + CO \tag{29}$$

All three are heterogeneous reactions, and each produces gaseous CO as a product. The thermodynamic equilibrium relationship between temperature of the system and pressure exerted by reaction products is shown in Fig. 2, which was prepared from information presented by Chipman[6] and Kubaschewski.[7] For the rapid reaction required in an ablation process, the gaseous reaction products must escape by exerting a pressure greater than that of the environment. In the case being modeled, the pressure of the environment corresponds to the stagnation pressure, which is assumed to be the pressure in the melt. Consider the history of a particle of glassy matter advancing toward the surface. It starts in a cool initial state and, as it moves, acquires a progressively higher temperature. Eventually it will reach the reaction temperature, since at some point along its path the temperature will be just sufficient for reaction to generate a pressure equal to that of the surroundings. Reference to Fig. 2 shows that reaction (27) is potentially capable of producing the highest pressures of the three reactions considered over the large range of temperatures from 1400°C, below which reaction (29) potentially would control, up to circa 2000°C, where reaction (28) potentially would control. These limits are obtained from noting intersections of lines on the plot which define highest attainable pressure level. Since it is anticipated that the 1400° to 2000°C temperature range will include the value of the predicted surface temperature, it is reaction (27) that is assumed to control.

Although these reactions potentially are capable of proceeding at the thermodynamic conditions just described, there is the matter of rates to consider. Accordingly, experiments were conducted to determine the speed of these reactions, and these were described in Ref. 1. It was found that rates were rapid at the temperatures of interest, although these experiments were conducted in vacua. It should be noted that these experiments in vacuum do not measure necessarily

the rate of reaction (27) in which silicon carbide forms. At pressures of a few microns, thermodynamics does not limit any of the reactions, even at 1300°C, as is evident from Fig. 2. However, as has been pointed out by Fulton and Chipman,[5] the slow step is probably either the breaking of the Si-O bonds or the slow removal of oxygen by carbon at the interface. Both these steps affect the rate of appearance of carbon monoxide in all three reactions almost equally. The mentioned experiments confirmed the adequacy of a first-order kinetics expression [see Eq. (3)] and provided numerical values for the constants k_R and ΔE given later.

For the purposes of this analysis, then, all the available evidence supports the contention that reaction (27) is controlling. This is not to say that the other reactions do not occur in hotter zones but is interpreted to mean that the sharply defined interface between reacting and nonreacting portions of the melt would exist as shown in Fig. 1 and that it corresponds to an interface of uniform temperature T_R. The equilibrium constant for this reaction is

$$K_a = \alpha_{SiC}\,\alpha_{CO^2}/\alpha_{SiO_2}\alpha_{C^3} \tag{30}$$

where α_{SiO}, α_{SiO_2}, and α_C are activity coefficients and are assumed equal to unity for these condensed materials. The α_{CO} equals its partial pressure p_{CO}, which in turn is equal to the stagnation pressure at the nose. K_a is a function only of temperature, and its dependence may be written as

$$\tfrac{1}{2}\log_{10}K_a = A - (B/T_R) = \log_{10}p_{CO} \tag{31}$$

The constant $2A$ is of the nature of an entropy change, whereas $2B$ is the enthalpy change for reactants to products, both in the standard states. The numerical value of the constants are $A = 8.71$ and $B = 15{,}100$ when T_R is in degrees Kelvin. The form of the equation and the numerical value of the constants follow from Fig. 2. Thus, when temperature distribution in the ablater is known, the depth at which reaction starts thereby is established, and this is the additional required relationship that is needed.

Aerodynamic Relationships

Up to this point, heat input and shear and pressure force distribution have been assumed to be known quantities. They may, in fact, be evaluated from some well-known correlations such as those due to Fay, Riddell, and Kemp[8] which are adopted now:

Heat Transfer

$$\frac{q_0}{h_s - h_i} = 0.7\left[(\rho\mu)_s\frac{du_e}{dx}\right]^{1/2}\sigma_s^{-2/3} \tag{32}$$

Shear Stress

$$\tau_0 = \frac{q_0(du_e/dx)}{h_s - h_i}\,x\,\sigma_s^{2/3} \tag{33}$$

These expressions relate the nonablative heat transfer rate q_0 and nonablative shear stress τ_0 to gas properties and flow conditions in the gas near the vicinity of the stagnation point. The pressure distribution is assumed Newtonian:

$$p = p_s[1 - (x^2/R^2)] \tag{34}$$

By application of Bernoulli's equation to a streamline at the outer edge of the boundary layer, (34) yields the following expression for the rate of change of tangential component of gas velocity along the direction of the surface:

$$\frac{du_e}{dx} = \frac{1}{R}\left(2\frac{p_s}{\rho_s}\right)^{1/2} \tag{35}$$

The same equation for pressure distribution, (34), also is used to evaluate $p''(0)$ for use in previous equations given in the foregoing.

To account for mass injection and its attendant effect on heat transfer and shear stress, the simple correlation previously used by Bethe and Adams[2] is adopted:

$$\psi = 1 - 0.67M^{0.25}(h_s - h_i)(\dot{m}/q_0) \tag{36}$$

where ψ represents the fractional amount of heat or of shear stress based on nonablative conditions which remains unblocked with mass addition. This equation states that the actual rate at which heat is blocked is a definite fraction of the rate at which enthalpy would be stored within the injected mass in bringing the injected mass from surface to the freestream condition. Thus,

$$q/q_0 = \tau/\tau_0 = \psi \tag{37}$$

The quantity $\dot{m}$ appearing in Eq. (36) is the rate of mass addition per unit surface area and is a function of the ablation material. For reinforced plastics there are two separate sources of gases that determine $\dot{m}$. M, the ratio of molecular weight of air to average molecular weight of injected species, is determined similarly. The two sources are pyrolysis gas, which is formed by thermal degradation of polymer at relatively low temperature, and inorganic reaction gas formed in the molten reaction zone. The pyrolysis gas is produced within the material at a depth greater than the liquid thickness. All the materials moving up with velocity v_∞ undergo pyrolysis. This material yields 11% by weight pyrolysis gas, and the gas has molecular weight of 9.8.[1] Let the percentage weight be represented by w and the molecular weight by $(MW)_p$.

The inorganic reaction gas is assumed to be an equimolar mixture of SiO and CO corresponding to stoichiometric combination of SiO_2 and C in equimolar amounts, and thus it has a molecular weight of 36. Actually, a typical material has about 30% of its original weight in excess glass. It was not felt important to include this fact in this description for two reasons. First, the model would become unwieldy, since reaction rates would become dependent on concentration and not merely on temperature as is now the case. Second, optimal behavior, corresponding to lowest ablation rate, corresponds to a stoichiometric mixture, since then the greatest use of chemical heat sinks as well as mass blocking is attained.

In view of the preceding discussion, the expression for $\dot{m}$ is as follows:

$$\dot{m} = \delta_R\,k_R\exp(-\Delta E/RT_R) + (w/100)v_\infty\rho \tag{38}$$

The average molecular weight MW is

$$\frac{1}{MW} = \frac{1}{\dot{m}}\left[\frac{1}{36}\,\delta_R\,k_R\exp\left(-\frac{\Delta E}{RT_R}\right) + \frac{1}{(MW)_p}\frac{w}{100}\,v_\infty\rho\right] \tag{39}$$

Thus the quantity M appearing in Eq. (36) is evaluated as follows:

$$M = 29/MW$$

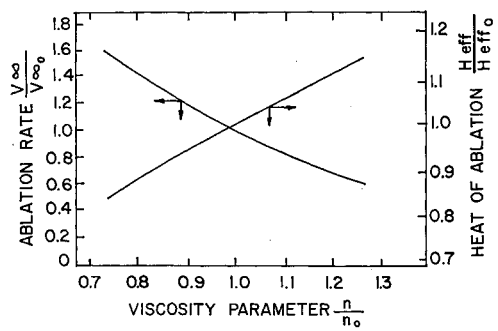

Fig. 3 Effect of viscosity on ablation rate.

The variable w is percent by weight of volatilized plastic material.

Computer Program

Numerical computations were done with the aid of a high-speed digital computer. Briefly, the procedure was as follows. A point in the re-entry trajectory is specified, and this determines aerodynamic conditions including stagnation pressure. From knowledge of the stagnation pressure, the reaction zone temperature is computed from Eq. (31). A value of v_∞ is guessed in (25) to start the solution; this allows δ_R to be computed and also leaves one additional equation, (24), to verify the guess. Convergence to five significant digits was obtained by a reiterative process. In the results presented below, w was set equal to zero, but finite w's are handled just as readily.

The calculated result for surface temperature was evaluated by a perturbation technique and furnished a test for the validity of the isothermal reaction layer assumption. The exact relationship for temperature distribution in the reaction layer even for the simple case when no gas is evolved and y direction velocity is constant is not obtainable in analytical form. Hence, an approximation technique was employed by assuming a form for the temperature profile. This profile is forced to satisfy certain boundary conditions, and so a reasonable prediction may be expected for the resultant description of the overall process. For simplicity, let the profile be assumed parabolic in shape:

$$T = C_1 + C_2 y + C_3 y^2 \tag{40}$$

where y has its previous meaning and denotes distance from the reaction-layer, melt-layer interface. Positive y is measured in the direction of the gas boundary layer, and material comes up from minus infinity. At $y = 0$, $T = T_R = C_1$, where T_R is determined from (31). Also at $y = 0$, the slope must be such that heat conducted out of the reaction layer equals heat supplied to the melt layer, or

$$k(\partial T/\partial y)_{y=0} = v_\infty \rho c_p (T_R - T_0) \tag{41}$$

Likewise, at the front surface, $k(\partial T/\partial y)_{y=\delta_R} = q$, where q is the net heat input from the boundary layer. This then determines, in Eq. (40),

$$C_2 = \frac{v_\infty \rho c_p}{k}(T_R - T_0) \qquad C_3 = \frac{q - v_\infty \rho c_p (T_R - T_0)}{2k\delta_R}$$

The temperature profile becomes

$$\left(\frac{T - T_R}{T_R - T_0}\right) = \frac{y}{\delta_T} + \left[\frac{q}{2K\delta_R(T_R - T_0)} - \frac{1}{2\delta_T\delta_R}\right] y^2 \tag{42}$$

The surface temperature T_s corresponds to $y = \delta_R$:

$$\left(\frac{T_s - T_R}{T_R - T_0}\right) = \frac{1}{2}\frac{\delta_R}{\delta_T} + \frac{q}{2k}\frac{\delta_R}{(T_R - T_0)} \tag{43}$$

Equation (43) was used to obtain a second estimate of surface temperature T_s, and a comparison of T_s and T_R was made for all cases run. The reaction layer was always thin, and T_s never differed by more than 6% from T_R (usually less than 1%), and hence the isothermal assumption is a legitimate one.

General Nature of Solutions

Some feel for the general response of the system was obtained by defining a reference set of conditions and then exploring perturbations of the solution in response to change in one independent parameter at a time. The results serve also to test the sensitivity of the answer to various physical input parameters, some of which may not be known to good accuracy and others of which vary with temperature but whose variance was not accounted for in the idealized model.

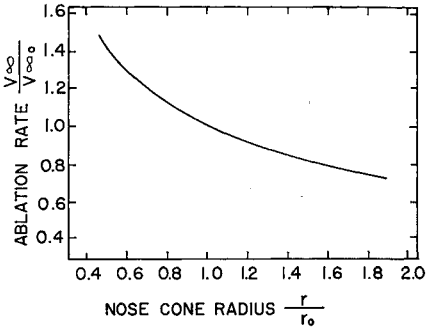

Fig. 4 Effect of nose cone radius on ablation rate.

The reference calculation was made with velocity, atmospheric, and physical parameters typical of an IRBM missile re-entry. Some of these parameters are as follows:

$M = 1.035$
$\sigma_s = 0.75$
$c_p = 0.35$ cal-g^{-1}-°K^{-1}
$h_i = (0.205\, T_R - 200)$ cal-g^{-1}
$R = 1.987$ cal-mol^{-1}-°K^{-1}
$\Delta E = 92{,}000$ cal-mol^{-1}
$k_R = 3.0 \times 10^{12}$ g-cm^{-3}-sec^{-1}
$\rho = 2.25$ g-cm^{-3}
$(k/\rho c_p) = 0.0076$ cm^2-sec^{-1}
$n = 16$
$\Delta H = 1420$ cal-g^{-1}
$T_0 = 540$°K

All results are reported in ratio to parameters corresponding to the reference case. The reference case results include the following values:

$T_s = 1922$°K
$T_R = 1920$°K
$q = 67.8$ cal-cm^{-2}-sec^{-1}
$\psi = 0.669$
$\delta_R = 0.000237$ cm
$\delta_T = 0.245$ cm

Specification of surface value of viscosity is of prime importance, and this was accomplished. The parameter n only specifies viscosities of cooler portions of the melt relative to the surface value. Figure 3 indicates a mild dependence of ablation rate on the numerical value of n. Since n is not truly a constant [see Eq. (14)], assumption of an average value results in roughly a 5% inaccuracy, as may be inferred from the graph and from knowledge of temperature within the material. Heat of ablation H_{eff} is defined in the usual manner as the heat transfer rate to a nonablating surface at the same temperature divided by the mass rate of material ablation, where both are based on a unit area of surface.

Figure 4 shows dependence of ablation rate on nose cone radius. As one would expect, the smaller radius nose ablates faster, this being caused by the overwhelming effect of increased heat flux, as Eq. (32) would indicate.

Figure 5 shows dependence of ablation rate on the reaction rate constant. It is seen that an increase in k_R over that assigned in the reference calculation ($k_R = 3.0 \times 10^{-12}$ g-cm^{-3}-sec^{-1}) does not increase the ablation rate appreciably further. The reaction rate "resistance" then may be said to have reached a limiting value, and the process is governed by other factors. One expects under these conditions that nearly all material entering the reaction zone would be reacted, leaving but a small fraction to flow away, and this situation is confirmed in the plot shown in Fig. 6.

Figure 7 shows the effect of chemical activation energy on the rate of ablation. The meaning of the curves corresponds to that discussed for Fig. 5, since changing ΔE is merely an alternate means of changing the total reaction rate.

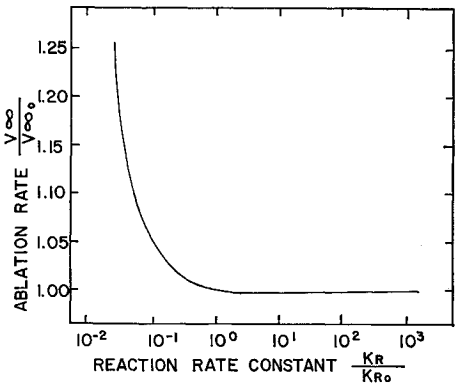

Fig. 5 Effect of reaction rate constant on ablation rate.

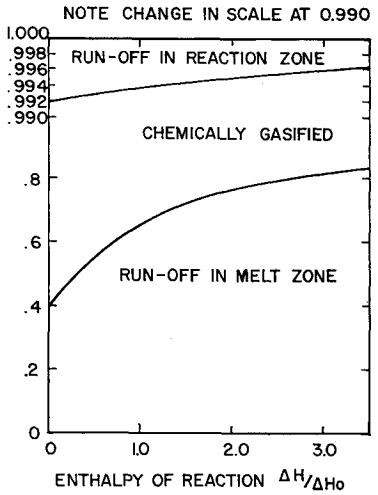

Fig. 6 Effect of increasing endothermicity of reaction on ablated - material balance.

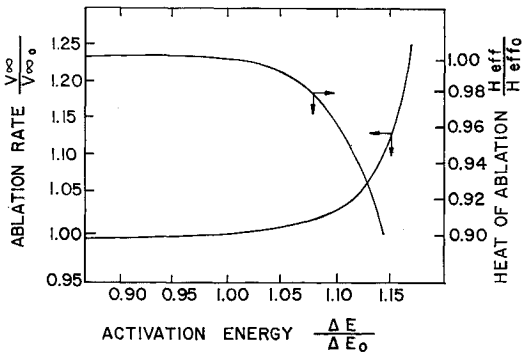

Fig. 7 Effect of activation energy of reaction on ablation rate.

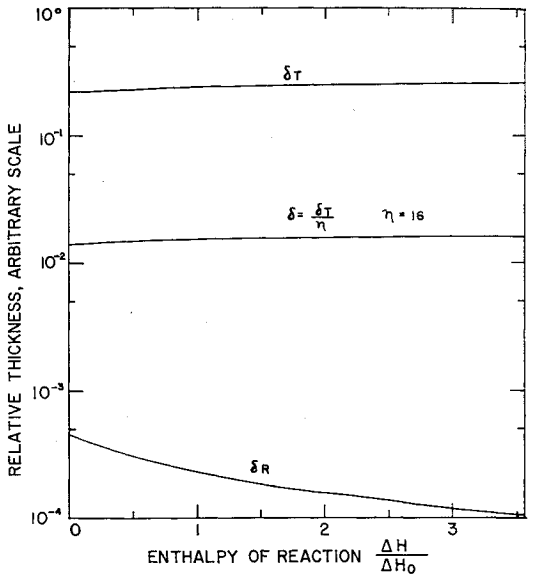

Fig. 8 Effect of reaction enthalpy on thickness of ablation process zones.

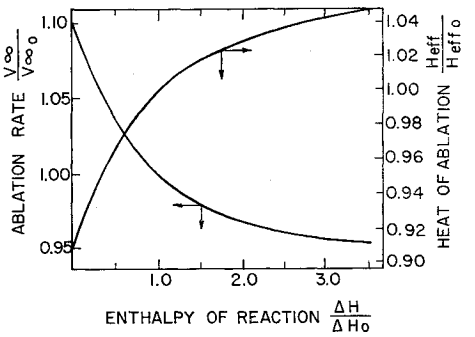

Fig. 9 Effect of reaction enthalpy on ablation rate.

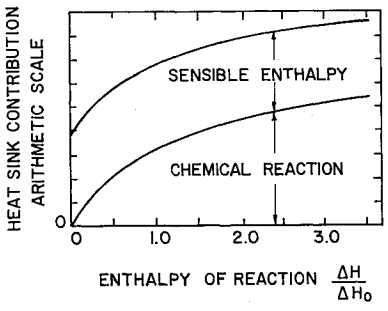

Fig. 10 Distribution of heat absorption as a function of reaction enthalpy.

Figures 6 and 8–10 relate the response of a variety of ablation parameters to change in enthalpy of the reaction. Figure 6 gives an accounting of the material balance. All material that ablates either runs off in the melt, reacts in the reaction zone, or runs off in the reaction zone. It is seen that the last-mentioned mechanism of material removal is a very minor one. Rather, nearly all material entering the reaction zone undergoes reaction. From 0.4 to 0.8 of total material ablated melts and flows off, never having reacted. This material may be considered to be ablated wastefully, since it did not react, and a large heat effect was unrealized. It is evident that any means of reducing this flow would improve the performance. Figure 8 compares thicknesses of the process zones. The theory predicts an exceedingly thin reaction zone. Supporting evidence is found in samples examined after re-entry; one observes a sharp surface of demarcation between carbonaceous substructure and the surface layer of excess glass which is found above it. Figure 9 shows the effect on overall ablation rate and the heat of ablation. Increasing ΔH reduces the ablation rate less than proportionally. A further indication of the fine response of the system is shown in Fig. 10, where the absorbed energy is classified further into that portion absorbed by chemical reaction as compared to the remainder that soaks into sensible enthalpy. Over the range of ΔH's on the graph, the fraction of heat blocked, given by ψ varies monotonically from 0.37 at $\Delta H = 0$ to 0.85 at the other extreme of the range of values.

It is evident that a self-consistent model has been described. Results of the calculation have been compared with a re-entry ablation rate. The calculated result underpredicted the observed peak ablation rate by about 38%. This would be impaired somewhat further if pyrolysis gas

were accounted for fully. Since the theory contained no adjustable constants, it is felt that the agreement is encouraging.

References

[1] Beecher, N. and Rosensweig, R. E., "Ablation mechanisms in plastics with inorganic reinforcement," ARS J. **31**, 532–539 (1961).

[2] Bethe, H. A. and Adams, M. C., "A theory for the ablation of glassy materials," Avco-Everett Research Lab., Res. Rept. 38 (November 1958).

[3] Sutton, G. W., "Hydrodynamics and heat conduction of a melting surface," J. Aerospace Sci. **25**, 29–32, 36 (1958).

[4] Hidalgo, H., "A theory of ablation of glassy materials for laminar and turbulent heating," Avco-Everett Research Lab., Res. Rept. 62 (June 1959).

[5] Fulton, J. C. and Chipman, J., "Kinetic factors in the reduction of silica from blast-furnace type slags," J. Am. Inst. Mining Met. Petrol. Engrs. **215**, 888 (1959).

[6] Chipman, J., "Thermodynamic properties of blast-furnace slags," *Metallurgical Society of AIME Conference on Physical Chemistry of Process Metallurgy* (Interscience Publishers, New York, 1961), p. 27.

[7] Kubaschewski, O. and Evans, E. L., *Metallurgical Thermochemistry* (John Wiley and Sons Inc., New York, 1956), Table E, p. 331.

[8] Fay, J. A., Riddell, F. R., and Kemp, N. H., "Stagnation point heat transfer in dissociated air flow," Jet Propulsion **27**, 672–674 (1957).

AUGUST 1963 AIAA JOURNAL VOL. 1, NO. 8

Structure of a Large-Radius Pinch Discharge

ROBERT G. JAHN* AND WOLDEMAR VON JASKOWSKY†
Princeton University, Princeton, N. J.

A large-radius pinch discharge produces a series of cylindrically symmetric, inwardly propagating current sheets and associated magnetic fields in a form convenient for detailed study of the $j \times B$ interactions basic to all schemes of electromagnetic gas acceleration. The discharge is examined by streak and Kerr cell photography, magnetic probes, spectroscopy, microwaves, and terminal measurements of current and voltage fluctuations, in order to determine the detailed distribution of the currents and fields as functions of radius and time. The initiation of the main discharge in a uniform peripheral ring is found to be primarily an inductive effect, conditioned somewhat by the presence of the adjacent insulator surface. Spectrograms of discharges in argon, nitrogen, and helium show singly and doubly ionized species indicating that particles of energy in excess of 25 ev are participating in the breakdown. A precursor front is observed to propagate ahead of the first current sheet and is identified tentatively as a gasdynamic shock. Another precursor, propagating many times faster, preionizes the gas slightly, prior to the arrival of the first current sheet.

I. Introduction

THE research described herein is directed toward an understanding of the initiation, development, and dynamic progress of the current sheets and associated magnetic fronts in a large-radius pinch discharge. The ultimate application is toward the efficient acceleration of an ambient body of gas for propulsion, but the present experiments are confined to the details of the discharge itself, with no attempt made to exhaust the plasma to generate thrust. The central apparatus is an aluminum discharge chamber with 8-in.-diam plane electrodes separated by a 2-in. gap of test gas. The discharge is driven by a circular bank of 15 1.0-μf capacitors charged to 10,000 v, ringing down through a low inductance circuit via a special gas-triggered switch described in detail elsewhere.[1] Figures 1 and 2 show a schematic drawing and a photograph of the circuit assembly.

The terminal electrical characteristics of the discharge are monitored by a current-measuring Rogowski coil encircling the switch column and a voltage divider applied across the main electrodes. From these it is found that the peak current in the discharge is about 200,000 amps, that the resonant frequency is about 250 kc, and that the total voltage developed across the chamber after breakdown is about 10% of that across the capacitors. It also is possible to infer the gross characteristics of the current distributions within the chamber as functions of time after breakdown.

The progress of the luminous patterns that develop within the chamber during the discharge are observed by rotating mirror streak photographs taken along a diameter of the chamber and by single-frame Kerr cell photographs taken at selected times. The details of the current density distributions are determined by small magnetic probes positioned at various radii inside the discharge chamber. Spectroscopic techniques provide information about the existence and development of various atomic and ionic species in the discharge, and 8- and 4-mm microwave probes monitor the development of the free electron density patterns. The

Presented at the AIAA Electric Propulsion Conference, Colorado Springs, Colo., March 11–13, 1963; revision received June 24, 1963. This work was supported by NASA Research Grant NsG-306-63. The authors wish to record their considerable indebtedness to several other workers in this field: A. E. Kunen and members of his staff at the Plasma Propulsion Laboratory of the Republic Aviation Corporation contributed substantially to the original design of the device and have been of continuing help throughout the course of the experiments. Of the many other contributors to our progress, we particularly have valued the advice and experience of R. H. Lovberg on several matters common to both his and our research efforts. Within our laboratory, A. L. Casini primarily has been responsible for the technical conduct of the experiments and for the many modifications and additions to the apparatus. N. A. Black, R. L. Burton, J. N. Corr, and W. R. Ellis have participated significantly in various phases of the program.

* Assistant Professor of Aeronautical Engineering. Member AIAA.

† Research Staff Member.